JOURNAL OF MATERIALS SCIENCE **34** (1999) 3659–3667

Experimental and theoretical study on the piezoelectric behavior of barium doped PZT

R. S. NASAR, M. CERQUEIRA
Departamento de Química, UFRN, Caixa Postal 1662, 59072-970 Natal-RN, Brazil

E. LONGO, E. R. LEITE
Laboratório Interdisciplinar de Eletroquímica e Cerâmica, Departamento de Química, UFSCar, Caixa Postal 676, 13565-São Carlos-SP, Brazil

J. A. VARELA
Instituto de Química, UNESP, Caixa Postal 355, 14800-900 Araraquara-SP, Brazil

A. BELTRÁN, J. ANDRÉS
Departament de Ciències Experimentals, Universitat Jaume I, Box 242, 12080 Castelló, Spain

An experimental and theoretical study of the ferroelectric and piezoelectric behavior of PZT doped with barium is presented. Ab initio perturbed ion calculations was carried out. The properties, such as remnant polarization, coercive field and the coupling factor of the PZT at constant sintering temperature was compared with the Zr^{4+}/Ti^{4+} ions dislocation energy and the lattice interaction energy. An agreement between the experimental and theoretical results, with a decrease of the interaction energy and an inversion of the energy stability from tetragonal to rhombohedral phase was observed. © *1999 Kluwer Academic Publishers*

1. Introduction

Lead Zirconate Titanate $Pb(Zr,Ti)O_3$ (PZT) is a solid solution between lead zirconate and lead titanate that presents ferroelectric and piezoelectric behavior and has important technological applications [1–7]. When the material has a nonsymmetrical structure, i.e. tetragonal, rhombohedral or orthorhombic its exhibits ferroelectricity, but becomes nonferroelectric (paraelectric) after a tetragonal to cubic transformation at the Curie temperature. The ferroelectric properties are known to originate from displacive transtations [8] of Ti^{4+}/Zr^{4+} cations between two stable off-centred sites of the TiO_6ZrO_6 octahedra, respectively, in response to an external field. The remnant polarization, Pr, and coercive field, E_c are intimately related to the deformation of the lattice [9]. The piezoelectric properties are dependent on the ratio of the starting materials, synthesis procedure, processing and doping methods [10–13]. However, the best piezoelectric properties of PZT (high dielectric constant, ε, and planar coupling factor, K_p) exist in the phase boundary between the tetragonal and rhombohedral phases, known as the morphotropic phase boundary (MPB) [14, 15].

Several authors agree about the first step of the mixed-oxide reaction route near the MPB which occurs by the reaction of PbO with TiO_2 to form $PbTiO_3$ [16] and the accepted route to yield the formation of both $PbTiO_3$ (PT) and $PbZrO_3$ (PZ) is the subsequent reaction to form a PZT solid solution [16–19]. The presence was also reported of an intermediate tetragonal solid solution of PbO with a small amount of TiO_2 and a trace of ZrO_2 [20, 21]. In this sense, Kulcsar [22] and Bernard [23] have observed that the addition of Ca^{2+} and Sr^{2+} in the Pb^{2+} position increases the K_p value.

Structural analysis of PZT solid solutions observed either a rhombohedral phase or a tetragonal phase at room temperature, depending on the composition ratio Zr/Ti, which are separated by a MPB [24]. The Zr^{4+} for Ti^{4+} substitutions in PT reduce the tetragonal distortion and ultimately cause the appearance of another ferroelectric phase such as rhombohedral R3m symmetry [25]. The increase of Zr^{4+} causes the appearance of the orthorhombic antiferroelectric phase near the Curie point. In the same sense, Jaffe *et al.* [9] consider that the tetragonal phase favour piezoelectric properties in opposition to the effect caused by the rhombohedral phase. Comes *et al.* [26], however, proposed that the polarization is dependent on crystallographic direction, the tetragonal phase consists of displacements along four cube diagonals, giving an average structure with a polarization along [100], whilst the rhombohedral phase is ordered along [111].

Cerqueira *et al.* [27] carried out lattice energy calculations for the tetragonal and rhombohedral structures using the aiPI method which showed a decrease in the stability of the tetragonal structure while the rhombohedral phase was stabilized until a concentration of 0.5 mol % calcium was achieved.

In the present work a combined experimental and theoretical study of the ferroelectric and piezoelectric behavior of PZT doped with barium is presented. In the theoretical part, the ab initio perturbed ion (aiPI)

methodology is used [28–30] in order to acquire an understanding of the relevant physical and chemical properties [31–35]. Following this we have investigated, from a theoretical point of view, the following aspects: (i) the effect of symmetrical displacements of the Ti^{4+} or Zr^{4+} ions along the *c*-axis, on the lattice energies of Ba^{2+} doped (0.25–1.5 mol %) tetragonal and rhombohedral PZT structures, and (ii) the evolution of the energy interactions as a function of the barium concentration.

In order to understand the ferroelectric and piezoelectric behavior of PZT-Ba, a comparison between our experimental and theoretical results is then carried out.

2. Experimental

The purity and origin of the raw materials were as follow: $Pb(NO_3)_2$ (99.3%-Merck); ZrO_2 (99.6%-Merck); TiO_2 (99.2%-Aldrich); Ba $(CH_3\text{-}COO)_2$ (99.2%-Reagen). A composition of $(Zr_{0.53}Ti_{0.47})O_2$ powder (ZT) was prepared by mixing and grinding zirconia and titania powders over 24 h in isopropyl alcohol. The powder was dried and then calcined at 1450 °C for 2 h. After calcination the material was deagglomerated in alumina mortar and then characterized by X-ray diffraction (Siemens model D-5000).

The solid solution ZT was diluted in water whilst stirring. A stoichiometric amount of lead nitrate was dissolved in this solution. To precipitate $Pb(OH)_2$ on the ZT particles NH_4OH was added until the pH reached the value of 11. The precipitate was washed, filtered and dried in an oven at 60 °C.

Calcium acetate was diluted in isopropyl alcohol and mixed with the precipitates $ZT + Pb(OH)_2$. The solution was stirred for 2 h and then dried, deagglomerated in a mortar and granulated in a 200 mesh screen. The amount of calcium acetate was calculated to give concentrations of 0.25, 0.50, 1.0 and 1.5 mol % relative to the precipitates.

This material was calcining at 850 °C for 2 h and the calcium doped PZT phases analyzed by the Rietveld method [36]. This method consists of comparing of the calculated X-ray diffraction patterns, obtained by defined crystallographic data, to the experimental X-ray diffraction pattern. The analysis is made by the least squares method.

Surface areas measured in the barium doped PZT were determined by nitrogen adsorption (model ASAP-2000 Micromeretics) and a value of 0.4 m^2/g^{-1} was found to be independent of the calcium concentration.

The powders were pressed into pellets of 12 mm diameter and about 2 mm thick by uniaxial pressing at 20 MPa. All compositions were sintered at 1150 °C for 3 h and characterized by X-ray diffraction pattern.

The PZT pellets of 0.25, 0.50, 1.0 and 1.5 mol % barium were polished back to 1 mm thick. Platinum electrodes were applied to the sample surfaces by sputtering. Electric fields in the range of 1.0 to 3.5 kV/mm were then applied to these samples for poling. The fundamental resonance frequencies were obtained using a complex impedance meter (model HP 4194 by Hewlett Packard).

3. Theoretical methods and models

3.1. Method

The aiPI method provides an adequate quantum mechanical treatment of the atom-in-the-lattice structure and has been presented by Luaña *et al.* [29, 30]; here we only summarize its main features.

According to the theory of electronic separability [37, 38], if a system can be partitioned into weakly interacting groups, its electronic wave function can be written as an antisymmetrized product of wave functions. If ΨA is the wave function of a particularly relevant group, i.e. the active (group), whose self-consistent-field (SCF) equations are solved in the field of the remaining (frozen) groups, the contributions of the A group to the total energy can be determined as an effective energy, E_{eff},

$$E^A_{\text{eff}} = E^A_{\text{net}} + \sum_{R(\neq A)} E^{AR}_{\text{int}} = E^A_{\text{net}} + E^A_{\text{int}}$$

which, by minimization, gives the best ΨA for a set of given frozen groups.

The effective energy arises from the contributions of the internal energy of the group, E_{net}, and the interaction energy, E_{int}, for this group with each of the ions in the lattice.

The total energy of the system is not the sum of the group effective energies. However, we can define the additive energy of group A as,

$$E^A_{\text{add}} = E^A_{\text{net}} + \tfrac{1}{2}E^A_{\text{int}}$$

For an $A_aB_bC_C\ldots$ Ionic crystal, the ions (A, B, C ...) are stabilized by the ion-lattice interaction energy, and the crystal energy per molecule is,

$$\begin{aligned} E_{\text{cryst}} &= aE^A_{\text{add}} + bE^B_{\text{add}} + cE^C_{\text{add}} + \cdots \\ &= aE^A_{\text{net}} + bE^B_{\text{net}} + cE^C_{\text{net}} + \cdots \\ &\quad + \tfrac{1}{2}\left(aE^A_{\text{int}} + bE^B_{\text{int}} + cE^C_{\text{int}} + \cdots\right) \end{aligned}$$

The lattice energy (E_{latt}) in the aiPi method is given by

$$E_{\text{latt}} = E_{\text{cryst}} - \left(aE^A_0 + bE^B_0 + cE^C_0 + \cdots\right)$$

Where the subscript stands for free-ion values.

3.2. Basis set representation

Large STO basis sets have been used on each atomic center 7s5p on Ba^{+2} and Ti^{+4}, 5s5p on O^{-2}, 10s9p5d on Zr^{+4} [39] and 12s8p6d2f on Pb^{+2} [40]. The optimization of the basis sets was carried out in order to minimize the total energy while maintaining SCF stability. The quantum mechanical contributions to the interaction energies have been considered for a large number of neighboring shells up to a convergence of 10^{-6} Hartrees in the crystal energy. The crystal energy, on the other hand, includes correlation estimated by means of the unrelaxed Coulomb–Hartree-Fock formalism [41]. It is termed unrelaxed because the aiPI wavefunctions are not affected by this correlation.

TABLE I

PZT	$0.53PbZrO_3$(PZ)/$0.47PbTiO_3$(PT)	$BaZrO_3$(BZ)/$BaTiO_3$ (BT)
0.25 Ba-PZT	(0.53–0.0125)PZ/(0.47–0.0125)PT	0.0125 BZ/0.0125 BT
0.50 Ba-PZT	(0.53–0.025)PZ/(0.47–0.025)PT	0.025 BZ/0.025 BT
1.00 Ba-PZT	(0.53–0.05)PZ/(0.47–0.05)PT	0.05 BZ/0.05 BT
1.50 Ba-PZT	(0.53–0.075)PZ/(0.47–0.075)PT	0.075 BZ/0.075 BT

Final composition = (0.5275PZ + 0.0125BZ) + (0.4675PT + 0.0125BT) = 0.25Ba-PZT(53/47).

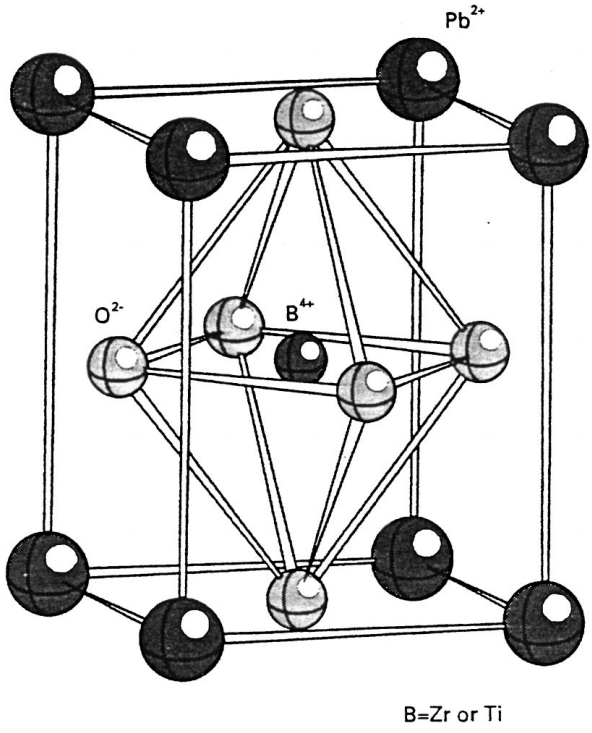

Figure 1 The PZT-Ba tetragonal structure.

The Madelung potential, responsible for the largest part of the interaction energies, has been analytically integrated. Layer by layer Ewald summation techniques were used to accurately sum long range Coulomb potential contributions.

3.3. Model

A schematic representation of the PZT tetragonal structure is depicted in Fig. 1. The PZT structure has been optimized by varying the Ti^{+4}/Zr^{+4} z-fractional coordinate for the rhombohedral (space group R3m) and tetragonal (space group P4mm) structures. The remaining structural parameters for pure and doped PZT, lattice and positional parameters, have been kept fixed at their experimental values obtained from X-ray diffraction experiments using the Rietveld method.

We have defined the polarization parameter as a measure of lattice stability, ΔE_s where the minimum lattice displacement energy (0 Å) is $E_{\min,T,R}$ and the maximum lattice displacement energy (0.05 Å) is $E_{\max,T,R}$ for both tetragonal and rhombohedral structures.

$$\Delta E_S = E_{\max,T,R} - E_{\min,T,R}$$

For the initial calculation an "infinity" crystal was considered, example: PZT(0.53 $PbZrO_3$/0.47 $PbTiO_3$). Following, for the representation of doping contribution in the structure, alleatory substitutions in this infinity crystal were carried out. Substitutions, such as barium in position of plumb at the same initial stoichiometry were carried out. Thus, Ba-PZT signify as shown in Table I.

4. Results and discussion

The powder analysis by X-ray diffraction of the PZT-Ba samples (Fig. 2), prepared by addition of barium acetate to ZT and $Pb(OH)_2$ mixtures in isopropyl alcohol and reacted by calcination at 850 °C and sintering at 1150 °C, shows that the barium oxide addition in the PZT (53/47) leads to the coexistence of tetragonal and rhombohedral phases.

According to Kakegawa and Mohri [42] the wet method used here leads to the formation of monophasic PZT near the tetragonal and rhombohedral phase boundaries. The coexistence of the phase is attributed to a compositional fluctuation of Zr^{4+} and Ti^{4+} ions in the PZT structure. Other authors [43] do not observe the coexistence of these two ferroelectric phases for materials prepared through the spray-dry process.

The phases quantity was analysed by the Rietveld method [36], (see Table II) and shows the rhombohedral phase appearance starting to 100% of tetragonal PZT phase. These results are coincident with those obtained by Kakegawa. The phase results demonstrated that the BaO addition leads the Tetragonal PZT phase to a compositional fluctuation with the phase diagram dislocation from a Ti^{4+} rich region to a region where tetragonal and rhombohedral phases coexist (MPB). The barium oxide addition to the PZT 53/47 changes the phase concentration ratio due to the formation of an intermediate phase $BaTiO_3$ that partially modifies the equilibrium towards the formation of the rhombohedral phase. It was observed that the relative density, (ρ/ρ_T, ρ = bulk density, ρ_T = theoretical density) increased with the addition of BaO.

Fig. 3, shows the ion-lattice interaction energy, Eint for each of the ions in the lattice as a function of Ba^{2+} concentration for the tetragonal and rhombohedral

TABLE II PZT-Ba with different concentrations. Relative density (ρ/ρ_0) and phases quantity

BaO (mol %)	$\rho/\rho t$	%Ft	%Fr
0	65	100	—
0.25	90	45	55
0.50	93	58	42
1.00	95	53	47
1.50	97	56	44

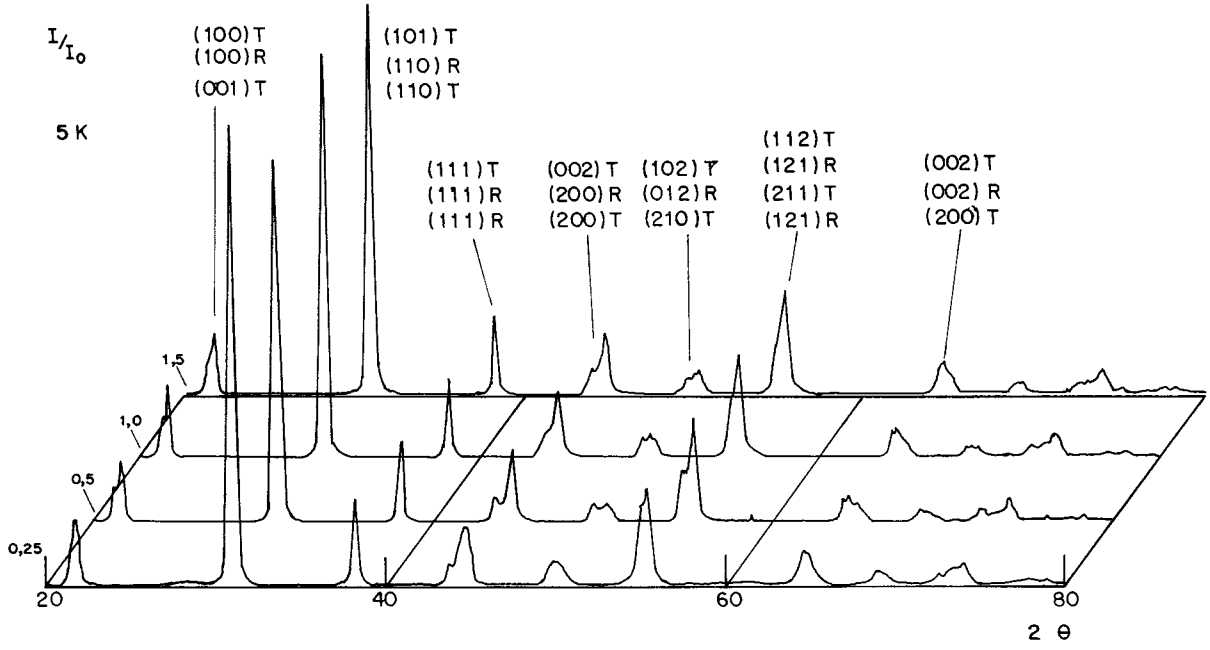

Figure 2 X-ray diffraction pattern of PZT-Ba sintered at 1150 °C/2 h. Rhombohedral and Tetragonal phases.

phases. An opposite trend with an increase of Ba^{2+} concentration in these two phases was observed. The lower repulsion was calculated for 0.25% barium concentration for the rhombohedral structure.

The ferroelectric characteristics show that the remnant polarization, Pr increased with the addition of BaO. The data analysis show different results from those obtained by Eyraud *et al.* [44] who shows values about 25 μm/cm^{-2} and was attributed to a decrease in the unit cell distortion. High values of the remnant polarization are directly related to the domain-wall motion and with Zr^{4+} and Ti^{4+} ion displacements in the unit cell. The energy barrier, Fig. 4 between two possible positions for the Zr^{4+}/Ti^{4+} moved by the action of an electric field is show. The potential barrier between 0 and 0.05 Å shows that the deformation energy of the rhombohedral structure is very superior to that observed on the tetragonal structure. In this way the strong local dipole formed in this structure doesn't leads to Zr^{4+}/Ti^{4+} ion mobility under small potentials.

The theoretical data analysis of the interaction energy, E_i was compared with experimental data of Pr, Fig. 5, which shows that the increase in the barium ion concentration contributed to the decrease in the energetic stability of the tetragonal and rhombohedral structures and thereby leads to low lattice stability and increases the Zr^{4+} and Ti^{4+} atoms displacement in the PZT crystal. In this sense, the energy barrier to Zr^{4+}/Ti^{4+} ion displacement is small and easily switching in the presence of the external electric field. The small stability of E_i leads to a dipole system that is poled easily by a low electric potential and this promoted an increase in the mobility increases of the ferroelectric domain-walls with the consequent Pr increase.

In schematic one-dimensional motion, the piezoelectric equation is $P = zd + E\chi$ where P is the polarization, z the stress, d the piezoelectric strain, E the field, χ the dielectric susceptibility, where d, E and χ are constants for a displacement in the lattice.

Ab initio aiPI calculations of the potential energy were carried out and show a parabolic potential as a function of Zr^{4+}/Ti^{4+} ion displacement in the perovskyte lattice. Such results are the same for different barium concentrations for both tetragonal and rhombohedral phases. These ionic displacements are reversed and after the electric field suppress the ions back to vibrate around its original positions. Despite being a small value, 0.05 Å, this displacement is much greater that generally occurring in solid ionic. This result, when associated with the 4+ charge of the Zr^{4+}/Ti^{4+} ions leads to a very high momentum in the unit cell.

Titanium and zirconium ions vibrate harmonically around their equilibrium positions at $z = 0$. The quantization condition of the energy levels to the harmonic oscillator is $E_n = (n + 1/2)h\nu$, where h is the Planck constant, ν frequency and n the quantum number $n = 0$, 1, 2, ...

Fig. 4, which shows the potential energy curve against z and with z variation (up to 0.05 Å) leading to an energy barrier to Zr^{4+}/Ti^{4+} ions by $\Delta E_s = E_{max,T,R} - E_{min,T,R}$, where $E_{min,T,R}$ is the zero point energy, $E_{max,T,R}$ is the $z = 0.05$ Å point energy and $\Delta E_s = nh\nu$. The vibrational frequencies were calculated, (see Table III), for Zr^{4+}/Ti^{4+} oscillations in the lattice.

The coercive field analysis, Fig. 6 shows a decrease relative to the PZT phase and shows a strong correlation between the BaO addition and the field. These

TABLE III Vibrational frequency of Zr^{4+} and Ti^{4+} ions in the PZT-Ba structure

0.05 Å	Ba concentration in PZT (mol %)			
	0.25	0.50	1.00	1.50
ν/n (cm^{-1})[a]				
Rhomb.	27461	21671	25273	24202
Tetrag.	9042	8368	9532	9683

[a] $n > 3$.

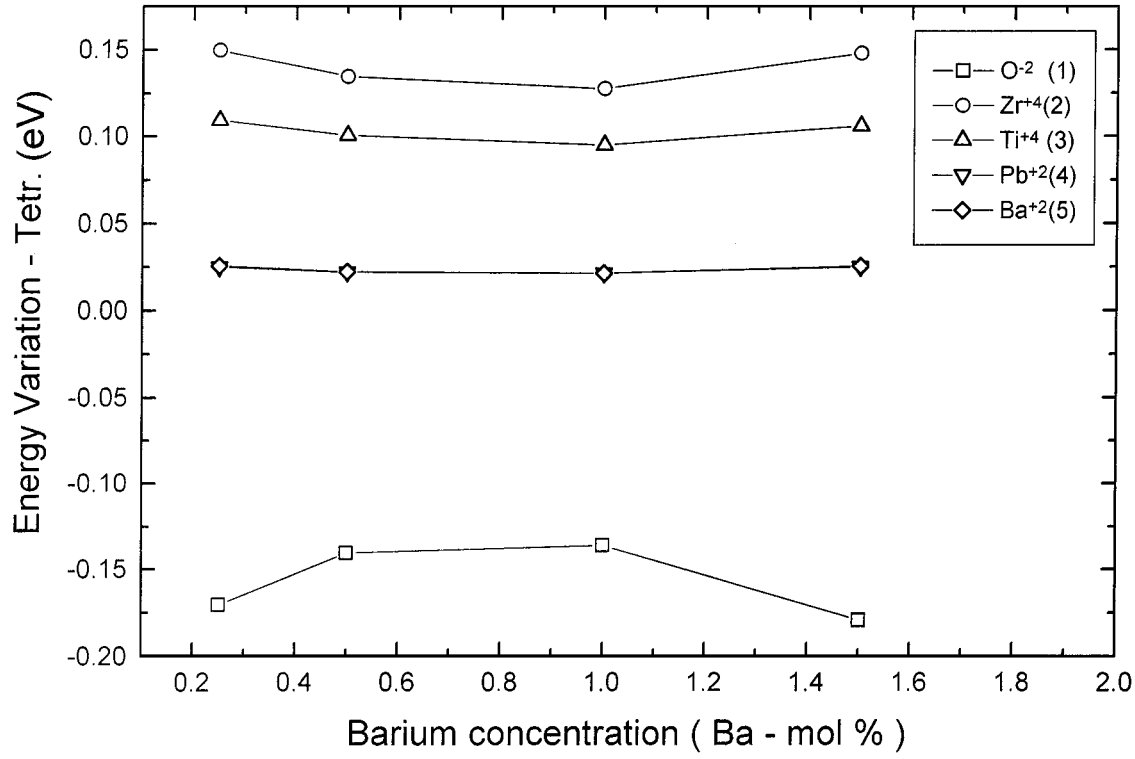

(a)

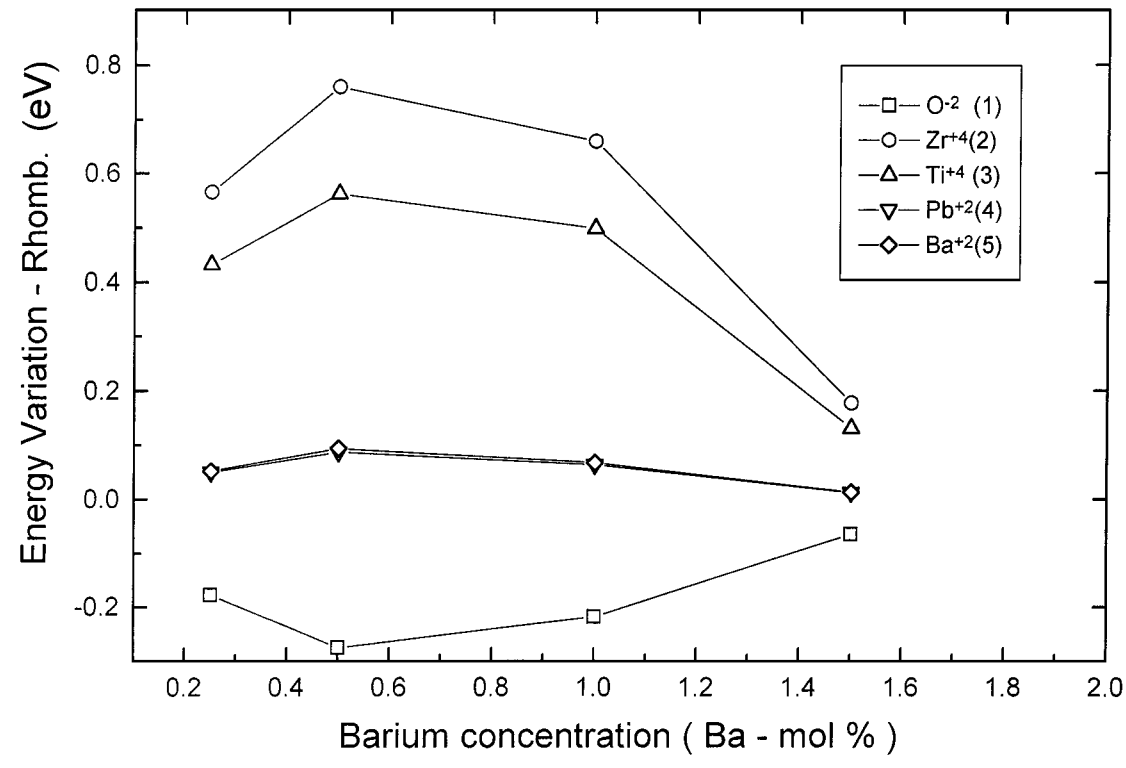

(b)

Figure 3 Variation of the ion-lattice energy, $E_{I\text{-}L}$, for each of the ions in the lattice as a function of the Ba^{2+} concentration for the (a) tetragonal and (b) rhombohedral phases (1) O^{2-}, (2) Zr^{4+}, (3) Ti^{4+}, (4) Pb^{2+}, (5) Ba^{2+}.

results demonstrated that low values near to $2E_c$ are necessary to switch the inversion domain of the polarization and promoted an electrically soft material. The E_c decreases show an agreement with the theoretical data. Major interaction energies lead to an increase in the Zr^{4+}/Ti^{4+} ion mobility and show that low energy is necessary to change the polarization sense and then the increases of barium concentration in the structure promoted the low potentials use to reverse the dipole sense ($>2E_c$).

The coupling coefficient results, Fig. 7 show a strong dependence on the increase in the barium addition. A decrease of the coupling factor with the additive concentration was observed. The coupling factor is strongly related to the internal friction of the material and its microstructural characteristics.

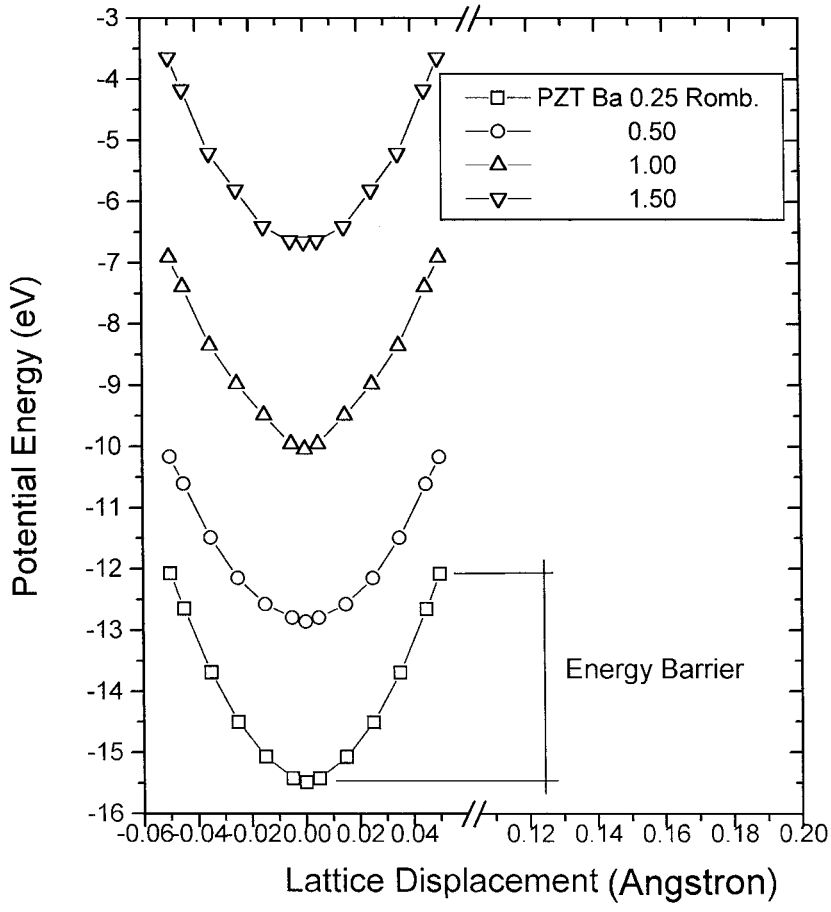

(a)

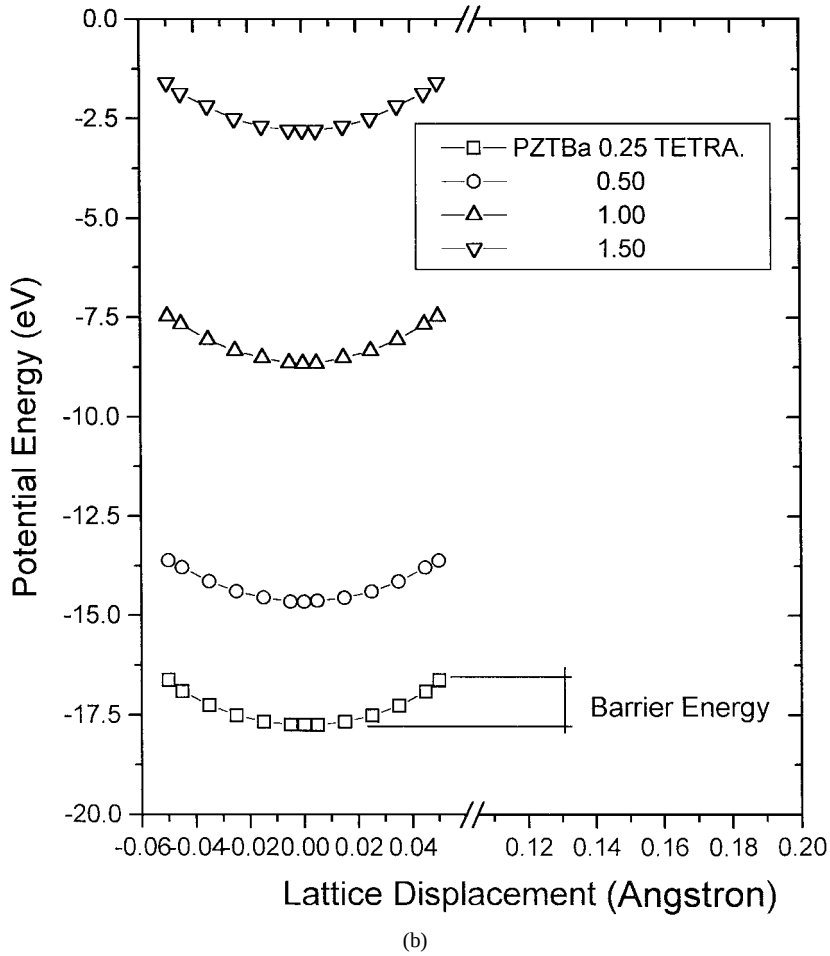

(b)

Figure 4 Potential energy against lattice displacement of Zr^{4+}/Ti^{4+} ions in the perovskite structure for the (a) rhombohedral phase (b) tetragonal phase.

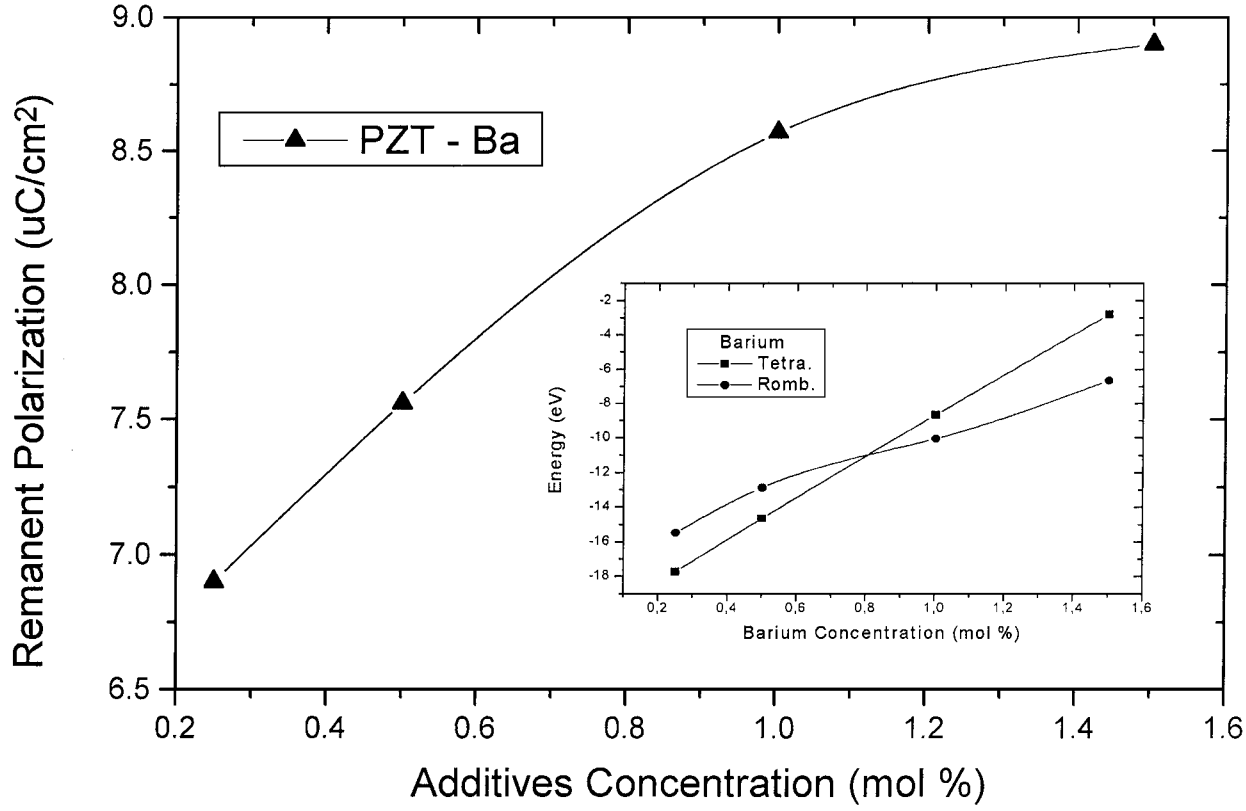

Figure 5 Remanent polarization against barium concentration and interaction energy against barium concentration (From tetragonal to rhombohedral reverse stability).

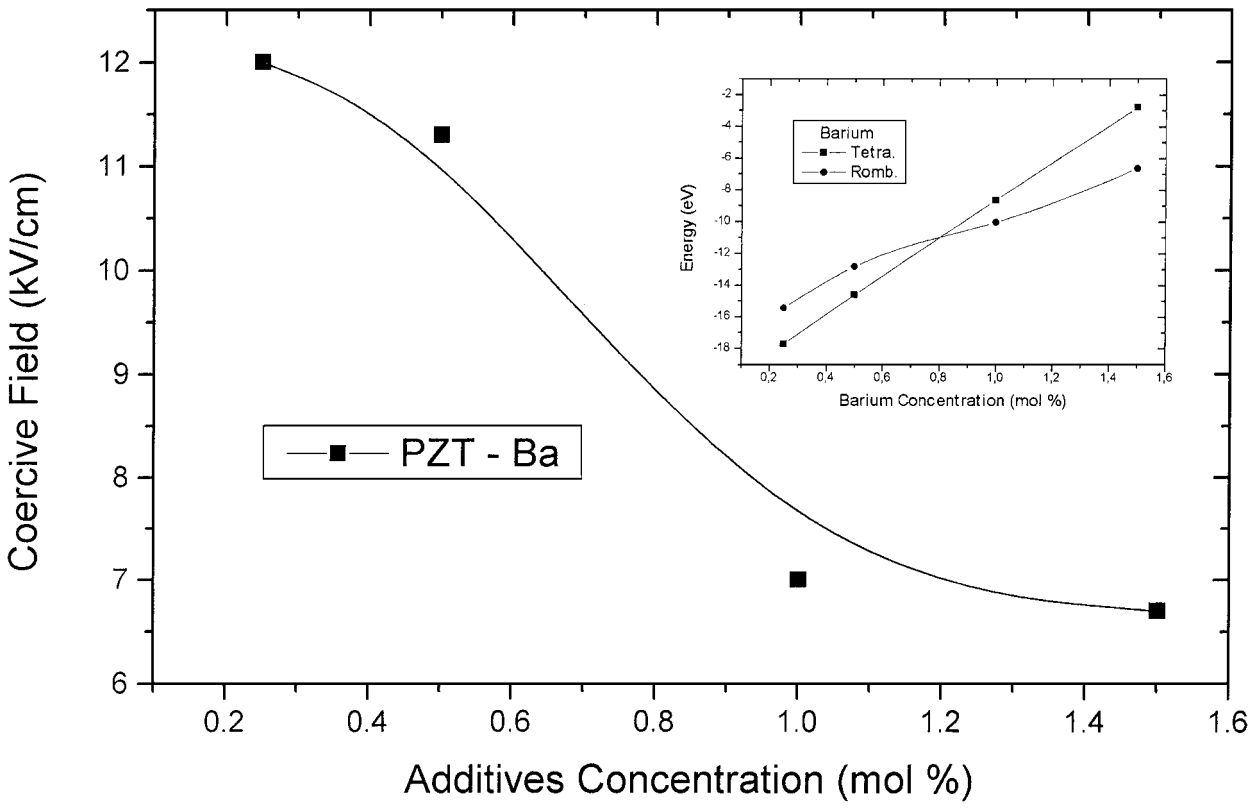

Figure 6 Coercive field against barium concentration.

The data analysis of the potential curve of Zr^{+4}/Ti^{+4} displacement shows that under low barium concentrations (~0.5 mol %) the unit cell polarization effect is stable in the tetragonal structure. Above this concentration a reversion occurs to the rhombohedral structure. The vibrational state of the rhombohedral structure, (Table II) presents a low vibrational mode relative to the tetragonal structure due to the interaction between the

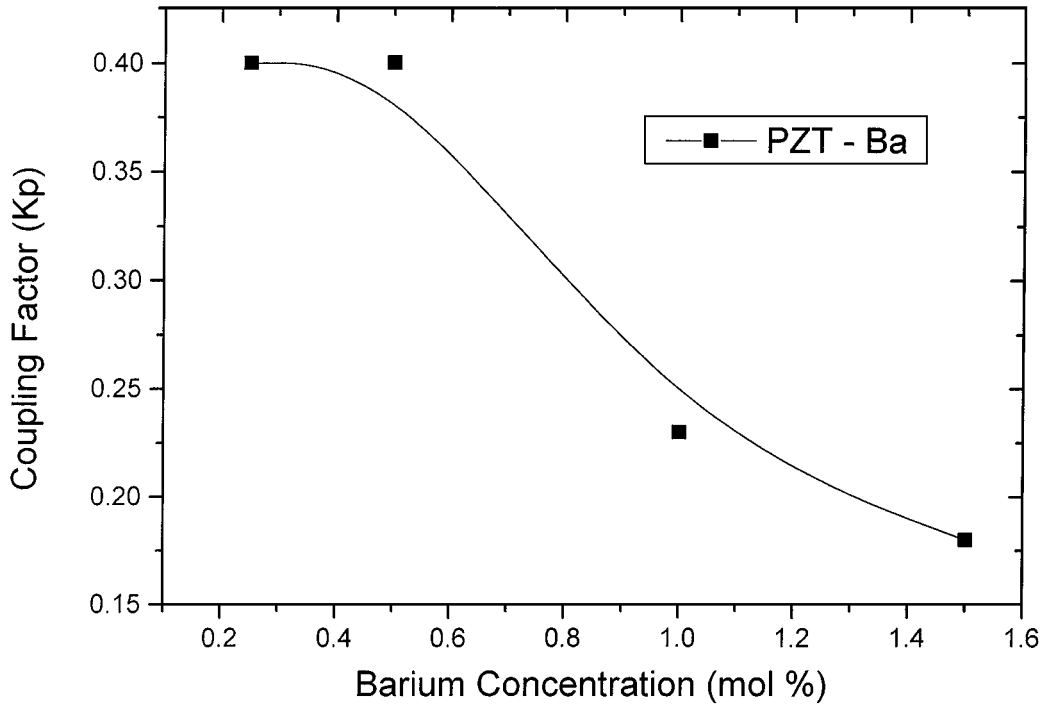

Figure 7 Coupling factor against barium concentration.

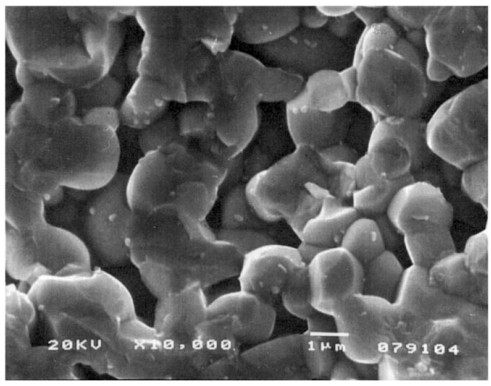

(a)

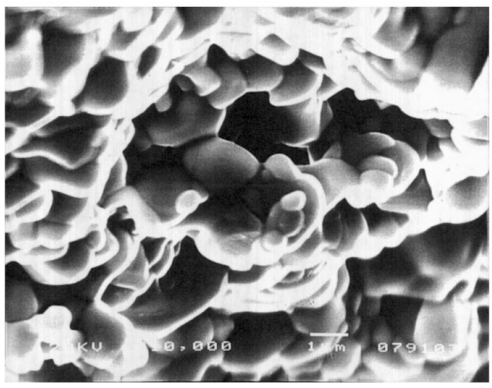

(b)

Figure 8 Microstructure of PZT-Ba sintered at 1150 °C/2 h (a) 0.25 mol % (×10,000); (b) 1.5 mol % (×10,000).

Zr^{4+}/Ti^{4+} atoms with the atoms of oxygen in octahedral position. These lattice characteristics would leads to a decrease in the transducer effect of the PZT-Ba.

The electron microscopy analysis, (Fig. 8) shows that there is a decrease in porosity with the increase in additive concentration. Factors such as size, shape and porosity alter the electrical properties of PZT. The coupling factor has a high dependence on the internal friction of the microstructure. The low piezoelectric efficiency of PZT-Ba with low concentrations cannot be attributed to density and microstructure factors considering that a density increases occurs and shows good grain size homogeneity.

5. Conclusions

A good agreement between the theoretical and experimental data was observed. The calculated interaction energy shows that Ba^{2+} ion additions leads to a decrease in the energetic stability of the tetragonal and rhombohedral structures. These results are associated with an increase of the remnant polarization and with a decrease in the coercive field.

The theoretical potential curve of the Zr^{4+}/Ti^{4+} dislocation shows an energy reversion from the tetragonal to the rhombohedral structure.

Acknowledgements

Financial support from the research founds of FAPESP and CNPq is gratefully acknowledged. We thank Dr. Victor Luanã for sending us the latest version of the aiPI method.

References

1. T. KAWAGUCHI. H. ADACHI, K. SETSUNE, O. YAMAZAKI and K. WASA, *Appl. Opt.* **23** (1984) 2187.
2. A. KUMADA, *Jpn. J. Appl. Phys.* **24** (1985) 739.
3. K. UCHINO, *Bull. Amer. Ceram. Soc.* **65** (1986) 647.
4. V. E. WOOD, J. R. BUSCH, S. D. M. RAMAMURTHI and S. L. SWARTZ, *J. Appl. Phys.* **71** (1992) 4557.
5. K. D. PRESTON and G. H. HAERTLING, *Appl. Phys. Lett.* **60** (1992) 2831.
6. C. C. HSUEH, T. TAMAGAWA, A. HELGELSON and D. L. POLLA, *Integr. Ferroelect.* **3** (1993) 21.

7. V. I. PETROVSKY, A. S. SIGOV and K. A. VOROTILOV, *ibid.* **3** (1993) 59.
8. E. M. LINES and A. M. GLASS, "Principles and Applications of Ferroelectrics and Related Materials" (Claredon, Oxford, 1977).
9. B. JAFFE, W. R. COOK and H. JAFFE, "Piezoelectric Ceramics" (Academic, New York, 1971).
10. S. NOMURA and S. SAWADA, *J. Phys. Soc. Jpn.* **10** (1955) 108.
11. O. YAMAGUCHI and H. MOGI, *J. Amer. Ceram. Soc.* **72** (1989) 1065.
12. T. YAMAMOTO, *Amer. Ceram. Soc. Bull.* **71** (1992) 978.
13. S. K. SAHA and D. AGRAWAL, *Integr. Ferroelect.* **71** (1992) 1424.
14. S. STOTZ, *Ferroelectrics* **76** (1987) 123.
15. A. V. TURIK, M. F. KUPRIYANOV, E. N. SIDORENKO and S. M. ZAITSEV, *Sov. Phys. Tech. Phys.* **25** (1987) 1251.
16. B. V. HIMERATH, A. I. KINGON and J. V. BIGGERS, *J. Amer. Ceram. Soc.* **66** (1983) 790.
17. T. OHMO, M. TAKAHASHI and N. TSUBOUCHI, *J. Jpn. Soc. Powder Metall.* **20** (1973) 154.
18. T. YAMAGUCHI, S. H. CHO, M. MAKAMORI and H. KUNO, *Ceram. Int.* **2** (1976) 76.
19. S. VENKATARAMANI and J. V. BIGGERS, *Amer. Ceram. Soc. Bull.* **59** (1980) 462.
20. Y. MATSUO and H. SASAKI, *J. Amer. Ceram. Soc.* **48** (1965) 289.
21. D. L. HANKEY, PhD thesis, Pennsylvania State University, 1980.
22. F. KULCSAR, *J. Amer. Ceram. Soc.* **42** (1959) 49.
23. J. BERNARD, "Piezoelectric Ceramics" (Academic, London, 1971).
24. F. VASILIU, G. LUCUTA and F. CONSTANTINESCU, *Phys. Status Solidi* **80** (1983) 637.
25. G. SHIRANE and K. SUZUKI, *J. Phys. Soc. Jpn.* **8** (1953) 615.
26. R. COMES, M. LAMBERT and A. GUINIER, *Acta Crystallogr.* **A26** (1970) 244.
27. M. CERQUEIRA, R. S. NASAR, E. LONGO, J. A. VARELA, A. BELTRAN, R. LLUSAR and J. ANDRÉS, *J. Mater. Sci.* **32** (1997) 2381.
28. V. LUAÑA and L. PUEYO, *J. Mol. Struct. (THEOCHEM)* **166** (1988) 215.
29. V. LUAÑA, F. RECIO and L. PUEYO, *Phys. Rev. B* **42** (1990) 1791.
30. M. FLÓREZ, E. FRANCISCO, V. LUAÑA, A. MARTIN-PENDAZ, J. M. RECIO, M. BERMEJO and L. PUEYO, in "Cluster Models for Surface and Bulk Phenomena" edited by G. Pacchioni, P. S. Bagus and F. Parmigiani (Plenum Press, New York, 1992) p. 605.
31. V. LUAÑA and L. PUEYO, *Phys. Rev. B* **41** (1990) 3800.
32. V. LUAÑA, M. FLOREZ, E. FRANCISCO, A. MARTIN-PENDÁS, J. M. RECIO, M. BERMEJO and L. PUEYO, in "Cluster Models for Surface and Bulk Fenomena" edited by G. Pacchioni, P. S. Bagus and F. Parmigiani (Plenum Press, New York, 1992) p. 619.
33. A. BELTRAN, A. FLORES-RIVEROS, J. A. IGUALADA, G. MONRÓS, J. ANDRÉS, V. LUAÑA and A. MARTÍN-PENDÁS, *J. Phys. Chem.* **97** (1993) 2555.
34. J. ANDRÉS, A. BELTRAN, J. CARDA and G. MONRÓS, *Int. J. Quantum Chem. Symp.* **27** (1993) 175.
35. J. ANDRÉS and A. BELTRÁN, *Chem. Phys. Lett.* **221** (1994) 249.
36. C. P. PAIVA-SANTOS, PhD thesis, IFQSc-USP 1990.
37. S. HUZINAGA and A. A. CANTU, *J. Chem. Phys.* **55** (1971) 5543.
38. V. LUAÑA and L. PUEYO, *Phys. Rev. B* **39** (1989) 11093.
39. E. CLEMENTI and C. RUETTI, *At. Data Nucl. Data Tables* **14** (1974) 177.
40. A. D. McLEAN and R. S. MCLEAN, *ibid.* **26** (1981) 197.
41. S. J. CHAKRAVORTY and E. CLEMENTI, *Phys. Rev. A* **39** (1989) 2290.
42. K. KAKEGAWA and J. A. MOHRI, *Solid State Commun.* **64** (1977) 769.
43. R. LAL and R. KRISHAN, *Br. Ceram. Trans. J.* **87** (1988) 99.
44. L. EYRAUD, P. EYRAUD, P. GONNARD and M. TROCCAZ, *Ferroelectrics* **31** (1981) 113.

Received 28 July 1998
and accepted 13 January 1999